Int. J. Heat Mass Transfer. Vol. 36, No. 16, pp. 3997–4008, 1993
Printed in Great Britain

0017–9310/93 $6.00 + 0.00

Temperature and penetration depth prediction for a three-dimensional field below a moving heat source

PETER EHRHARD, CHRISTOPH HÖLLE and CHRISTIAN KARCHER
Kernforschungszentrum Karlsruhe GmbH, Institut für Angewandte Thermo- und Fluiddynamik, Postfach 3640, D-76021 Karlsruhe, Germany

(*Received* 21 *December* 1992 *and in final form* 16 *March* 1993)

Abstract—Predictions for both penetration depth of a specific isotherm and for peak temperatures achieved during processing of brick-type workpieces are inferred. A rectangular heated area is thereby travelled at constant speed across the top surface of the workpiece. The model accounts for the finite cross-track extents of the workpiece as well as for a realistic heat transfer towards an underlying table. The model is strictly valid for conduction-dominated processes. New results are obtained for cases where, due to geometry of workpiece and heated area, truly three-dimensional heat flow situations are present. This is particularly relevant, when the bottom plane's heat losses or the limiting side planes have a considerable influence on the heat flow. Moreover, it is explored which parameter ranges allow reasonable predictions by using simplified models, as given by several previous studies.

1. INTRODUCTION

LASER surface treatment of metallic substrates is considered more and more as an applicable—but still expensive—industrial process to realize desired physical or chemical qualities just at the surface of a workpiece. Techniques hereby may be based on pure solid-state transformation or may involve solid/liquid phase changes of the substrate material. A review of such techniques has been recently given by, e.g. Mazumder [1] or Molian [2]. Independent of the specific process, a prediction of the process parameters is of vital interest to minimize the number of (expensive) tests.

In the present article we focus on processes which are dominated by conduction. Examples of such processes are transformation hardening, annealing, or any melting processes such as surface alloying, hard particle incorporation, etc., as long as the flow inside the molten region develops only weak contributions to the heat transport. That is usually the case if only small molten zones are present and/or if the driving mechanism of the flow is weak. For such processes the result (and success) of the treatment is determined by the penetration depth of a specific temperature (e.g. transformation or melting temperature) and the peak temperature achieved during processing. Predictions of the processing parameters, therefore, are required to develop correlations between those crucial quantities and the adjustable parameters at the lasering machine. These are the laser power, the scanning speed, the geometry and power distribution of the laser spot and, as we shall see later on, probably the thermal contact of workpiece and the underlying table.

There are many previous studies in the literature, both experimental and theoretical, which aim to derive predictions for the above described type of processes. We shall restrict ourselves in the the following review to studies with conduction as the dominant mechanism. In probably the most fundamental paper Rosenthal [3] applies the classical methods, as catalogued, e.g. by Carslaw and Jaeger [4], to metal treatment processes. Thus, he derives a number of closed-form solutions for the temperature field below a moving heat source for certain sets of (idealistic) boundary conditions. The principles of treating workpieces of finite width or thickness are likewise developed. Examples for further analytical approaches are Cline and Anthony [5], who derive predictions for a circular Gaussian heat source, travelling across a semi-infinite workpiece, or Ashby and Easterling [6], who develop predictions based on approximate solutions for identical conditions. In a more recent paper Shercliff and Ashby [7] bring together approximative closed-form solutions and a large number of experimental data to derive and verify a so-called 'master diagram'. Their results, likewise valid for semi-infinite workpieces, allow for predictions of engineering utility, since a careful test against a large number of previous models and experiments ensures validity in a wide parameter range. A study of similar flavour was conducted by Steen *et al.* [8], who employ a one-dimensional conduction balance below a scanning line source to derive predictions for the penetration depth of a specific temperature into a semi-infinite workpiece. Again, tests of this 'simple' model against their experiments and against Shercliff and Ashby [7] on the one hand, and against fully numerical (FEM) simulations on the other hand, demonstrate the range of validity of their

NOMENCLATURE

b, h	width and thickness of the workpiece
d, a	size of heat source in scanning and cross-track direction
c_p	specific heat of workpiece material
k	heat transfer coefficient (bottom plane)
Nu	Nusselt number
Pe	Peclet number
q	net absorbed power density
Q	net absorbed power
t	time
t^*	penetration depth
T	local temperature
T_∞	ambient (initial) temperature
$\hat{T}$	peak temperature
T^*	penetrating temperature
U	scanning velocity of heat source
$\mathbf{v}$	velocity vector
x, y, z	fixed Cartesian coordinates
x_h	position of heat source centre
X, Y, Z	moving Cartesian coordinates in dimensionless form.

Greek symbols

η	number of point sources in Z
θ	dimensionless temperature
θ^*	dimensionless penetrating temperature
κ	thermal diffusivity of workpiece material
λ	heat conductivity of workpiece material
ρ	density of workpiece material
τ	dimensionless time
ω	number of point sources in X.

predictions. Moreover, necessary conditions for the semi-infinite assumption are derived.

A similar objective, namely the derivation of simplified models suitable for industrial users, is the subject of two studies of Festa *et al.* [9, 10]. They analyze the two-dimensional heat flow problem below a moving line source in a semi-infinite body and predict maximum temperatures and hardening depths. They demonstrate a simplified (one-dimensional) model to reveal reasonably-accurate predictions for large scanning rates. Similar conclusions are drawn within a paper of Timans *et al.* [11], for the identical problem. These authors give, additionally, conditions for the width of the line source.

There are likewise fully numerical studies within the literature. Kou *et al.* [12] develop a finite-difference model for the three-dimensional heat flow in a semi-infinite body below a rectangular moving heat source. Kou [13], moreover, shortly considers both the problem of finite width and finite thickness of the workpiece, without presenting results for these particular cases. He suggests an adiabatic boundary condition at the side planes and a third-type boundary condition at the bottom plane under those circumstances.

There are several deficiencies up to the present as far as really three-dimensional heat flow situations are concerned, i.e. situations where a workpiece of finite width and finite thickness is present, generally exposed to a heat source of different measure. Moreover, a workpiece is typically positioned upon a table and, due to the finite thickness of the workpiece, the heat flux into the table may become an important issue. To summarize, there are few predictions available if the semi-infinite assumption, the infinite thickness assumption, idealistic boundary conditions or two-dimensional models are not appropriate.

The aim of the present paper, therefore, is to develop predictions for (a) the penetration depth of a specific temperature and (b) the peak temperature, as the most significant quantities during processing (cf. Festa *et al.* [9]). Brick-type workpieces of infinite length but finite thickness and width are the focus, while in general a three-dimensional heat flow is present. The heat flux through the bottom plane into the table is particularly investigated, while a control of the process by means of the control of the thermal contact of workpiece and table is envisioned. All predictions are developed by means of numerical (FEM) simulations and, in the case of meaningful limits, by closed-form models extending Rosenthal's [3] ideas. Finally, we aim to demonstrate in which parameter ranges the use of more idealized models (cf. [7–10]) proves to reveal reasonable predictions.

2. FORMULATION

In Fig. 1 the problem is sketched. We consider a brick-type workpiece of infinite extent in scanning direction x, thickness h and width b. At the top surface a rectangularly-shaped heat source (e.g. a laser spot) with net power density q is travelling at a constant speed U parallel to the x-axis. The workpiece is sur-

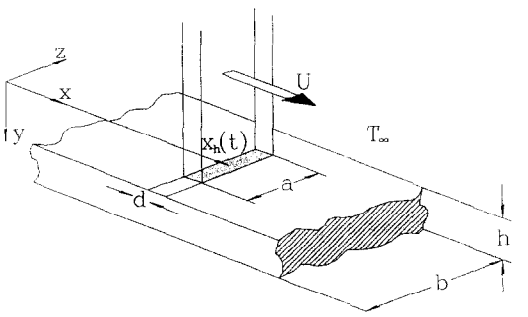

FIG. 1. Sketch of the problem geometry.

rounded by an ambient atmosphere of gas at constant temperature T_∞ and placed upon a table.

Within the fixed coordinate system (x, y, z) the temperature field in the solid is governed by the heat transport equation

$$\rho c_p \left\{ \frac{\partial T}{\partial t} + (\mathbf{v}\cdot\nabla)T \right\} = \lambda \nabla^2 T, \tag{1}$$

together with the appropriate set of boundary conditions, namely

$$x \to +\infty, y, z: \quad \frac{\partial T}{\partial x} = 0, T = T_\infty, \tag{2}$$

$$x \to -\infty, y, z: \quad \frac{\partial T}{\partial x} = 0, \tag{3}$$

$$x, y = h, z: \quad \frac{\partial T}{\partial y} = -\frac{k}{\lambda}(T - T_\infty), \tag{4}$$

$$|x - x_h| > \frac{d}{2}, y = 0, z: \quad \frac{\partial T}{\partial y} = 0, \tag{5}$$

$$|x - x_h| \leqslant \frac{d}{2}, y = 0, |z| \leqslant \frac{a}{2}: \quad \frac{\partial T}{\partial y} = -\frac{q}{\lambda}, \tag{6}$$

$$|x - x_h| \leqslant \frac{d}{2}, y = 0, |z| > \frac{a}{2}: \quad \frac{\partial T}{\partial y} = 0, \tag{7}$$

$$x, y, |z| = \frac{b}{2}: \quad \frac{\partial T}{\partial z} = 0. \tag{8}$$

Thus, we approximate the workpiece bounded by essentially adiabatic planes, except for the bottom plane and the top plane's heat source area. The heat source area features a constant heat flux boundary condition as produced by the new absorbed power density q. The bottom plane is modelled, following Kou [13], using a third-type boundary condition. This boundary condition allows, through the heat transfer coefficient k, to adjust the complex heat transfer conditions resulting through contact between the workpiece and the table. We neglect in our analysis, for benefit of transparency, any heat losses through the top plane or the side planes, which might be present due to radiative and/or convective effects. It turns out, however, that those heat fluxes have only minor importance for typical applications, as, e.g. laser surface processing of steel. In contrast, heat losses through the bottom plane into the usually well-conducting table as well as advective heat losses due to the source movement dominate the conduction problem inside the workpiece. Thus, the above model (1)–(8) preserves the most important effects present during typical technical processes.

The above formulation (1) in fixed coordinates leads to a time-dependent problem due to the time-dependent position of the heat source $x_h(t)$ within the boundary conditions (5)–(7). Within the next step we therefore transform to a moving, source-attached coordinate system in conjunction with an appropriate scaling. The spatial coordinates (x, y, z) are transformed using

$$(X, Y, Z) = \frac{1}{h}\Big[(x + Ut), y, z\Big], \tag{9}$$

while we employ a conductive temperature scale and an interaction time scale, i.e.

$$\theta = \frac{(T - T_\infty)\lambda}{qh}, \quad \tau = \frac{tU}{h}. \tag{10}$$

By introducing (9) and (10) into the basic equation and boundary conditions (1)–(8) we find the dimensionless formulation within a moving reference frame (X, Y, Z), namely

$$\frac{\partial \theta}{\partial \tau} + (-1)\frac{\partial \theta}{\partial X} = Pe^{-1}\left\{ \frac{\partial^2 \theta}{\partial X^2} + \frac{\partial^2 \theta}{\partial Y^2} + \frac{\partial^2 \theta}{\partial Z^2} \right\}, \tag{11}$$

$$X \to +\infty, Y, Z: \quad \frac{\partial \theta}{\partial X} = 0, \theta = 0, \tag{12}$$

$$X \to -\infty, Y, Z: \quad \frac{\partial \theta}{\partial X} = 0, \tag{13}$$

$$X, Y = 1, Z: \quad \frac{\partial \theta}{\partial Y} = -Nu\theta, \tag{14}$$

$$|X| > \frac{d}{2h}, Y = 0, Z: \quad \frac{\partial \theta}{\partial Y} = 0, \tag{15}$$

$$|X| \leqslant \frac{d}{2h}, Y = 0, |Z| \leqslant \frac{a}{2h}: \quad \frac{\partial \theta}{\partial Y} = -1, \tag{16}$$

$$|X| \leqslant \frac{d}{2h}, Y = 0, |Z| > \frac{a}{2h}: \quad \frac{\partial \theta}{\partial Y} = 0, \tag{17}$$

$$X, Y, |Z| = \frac{b}{2h}: \quad \frac{\partial \theta}{\partial Z} = 0. \tag{18}$$

The above set of equations (11)–(18) involves certain dimensionless groups. The Peclet number Pe ratios heat transport by advection and heat transport by conduction. The Nusselt number Nu characterizes the heat transfer towards the table, i.e. the boundary condition at the bottom plane. The limiting situations are $Nu \to 0$, which gives the adiabatic boundary condition, and $Nu \to \infty$, which corresponds to a perfectly-conducting (constant temperature) boundary condition. The definition of these groups is

$$Pe = \frac{Uh}{\kappa}, \quad Nu = \frac{kh}{\lambda}. \tag{19}$$

The above dimensionless formulation, except for the characteristic length h, resembles that of Chan *et al.* [14] used within the context of a combined solid/liquid problem.

2.1. *Similarity analysis*

Given the above dimensionless formulation of the problem (11)–(18) we recognize a total of 5 dimensionless groups Π_i entering the solution for the tem-

perature field $\theta(X, Y, Z)$. These are the geometry parameters

$$\Pi_1 = \frac{b}{h}, \quad \Pi_2 = \frac{d}{h}, \quad \Pi_3 = \frac{a}{h}, \tag{20}$$

as well as the Peclet and Nusselt numbers

$$\Pi_4 = Pe, \quad \Pi_5 = Nu. \tag{21}$$

Therefore, for the temperature field θ we expect the dependency

$$\theta(X, Y, Z) = f\left(\frac{b}{h}, \frac{d}{h}, \frac{a}{h}; Pe, Nu\right). \tag{22}$$

At first sight it seems paradoxical that the power density q does not enter one of the dimensionless groups Π_i. By calculating the temperature field in physical units $T(x, y, z)$ using equation (10) we recognize the role of q as it scales temperature through the reference value (qh/λ).

There are several quantities which represent an important piece of information for the control of any surface treatment process. These are in particular the penetration depth t^* of a specific temperature T^*, which might correspond to a transformation, hardening or melting temperature. Moreover, the maximum temperature $\hat{T}$ achieved during processing is of interest.

If we aim to predict the penetration depth t^*, this in general, can be extracted from a quasi-stationary solution for the temperature field. This statement holds if the extent of the workpiece in the scanning direction x is sufficiently large (cf. Bornefeld [15]). Thus, the penetration depth t^* depends as

$$\frac{t^*}{h} = f\left(\frac{b}{h}, \frac{d}{h}, \frac{a}{h}; Pe, Nu, \theta^*\right), \tag{23}$$

wherein θ^* is the dimensionless version of the respective temperature T^*, using equation (10). Through θ^* the dependency of the penetration depth on the power density q is recovered, as expected. Finally the maximum temperature $\hat{T}$ is directly available from the temperature field at the top $(Y = 0)$ of the centre cross section $(Z = 0)$ of the workpiece, i.e. we have

$$\hat{T} = T_\infty + \frac{qh}{\lambda} \mathrm{MAX}\{\theta(X, Y = 0, Z = 0)\} = T_\infty + \frac{qh}{\lambda}\hat{\theta}, \tag{24}$$

and therefore the dependency is

$$\hat{\theta} = \lambda \frac{(\hat{T} - T_\infty)}{qh} = f\left(\frac{b}{h}, \frac{d}{h}, \frac{a}{h}; Pe, Nu\right). \tag{25}$$

3. SOLUTION METHOD

There are several situations for which quasi-stationary analytical solutions for the temperature field can be developed, as demonstrated by Rosenthal [3] or Carslaw and Jaeger [4]. These solutions, for the case of a heat source line or area, may be based on approximating the heat source distribution by a finite or infinite number of point sources, distributed in an appropriate manner at the top plane of the workpiece. The first approach leads to a finite series representing the source term. Although temperature is singular at the position of each single source, this approximation reveals physically correct results for the global heat balance, i.e. in a sufficiently large distance from the source positions. It is clear that by increasing the number of point heat sources the accuracy of the solution is improved. The second approach leads to an integral formulation of the source term as demonstrated by Rosenthal [3]. We employ, indeed, finite series further on to model the heat source area. Even though difficulties may arise for predictions of very small penetration depths, this method saves an enormous amount of computing time.

The above approximations as such both give analytical solutions valid for a semi-infinite workpiece, characterized by $h \to \infty$ and $b \to \infty$. To fulfill the desired boundary conditions at the side and bottom planes of the workpiece, the so-called 'method of images' can additionally be employed (cf. Rosenthal [3]). An infinite number of fictitious sources is arranged such that planes parallel to the scanning direction exhibit certain symmetries. This method does not, of course, apply to planes perpendicular to the source movement. Therefore, we remain restricted to a workpiece of infinite extent in X.

Within the following sections we shall develop three different approximate solutions in order to access temperature fields for certain relevant situations analytically. Finally, a fully-numerical solution of the most general problem on base of finite elements is given.

3.1. *Workpiece of infinite thickness*

The simplest solution relevant to the problem given in Fig. 1 takes account of the finite width b of the workpiece and allows us to pose the adiabatic boundary condition (18) at the side planes. In the y-direction, however, the boundary condition

$$X, Y \to +\infty, Z: \quad \frac{\partial \theta}{\partial Y} = 0 \tag{26}$$

replaces boundary condition (14) at the bottom plane. The temperature field obtained for this situation corresponds to a workpiece which extends in depth to infinity. The physical boundary of the workpiece at the bottom plane $(Y = 1)$ therefore does not have any influence on the temperature field. In practice such a situation may occur if the workpiece is in good contact with a thick table of similar thermophysical properties and/or if the workpiece thickness h is large. By a comparison of time scales, namely interaction time d/U should be sufficiently smaller than thermal diffusion time h^2/κ, Steen *et al.* [8] have derived a criterion for the validity of the semi-infinite workpiece

assumption, which should likewise hold for infinitely thick workpieces. Transferred into the present notation they give

$$\frac{h}{d} \gg \frac{1}{Pe}. \tag{27}$$

The temperature field for this infinite thick workpiece is given by

$$\theta(X, Y, Z) = \frac{ad}{2\pi\omega\eta h^2} \sum_{\nu=1}^{\omega} \left\{ \exp\left[-\frac{Pe}{2}(X - X_\nu) \right] \times \sum_{\mu=1}^{\eta} \sum_{n=-\infty}^{+\infty} \frac{\exp\left[-\frac{Pe}{2} R_n \right]}{R_n} \right\},$$

with

$$R_n = \left((X - X_\nu)^2 + Y^2 + \left(Z - Z_\mu - \frac{b}{h} n \right)^2 \right)^{1/2},$$

$$X_\nu = \frac{d}{2h}\left[\frac{2(\nu - 1)}{(\omega - 1)} - 1 \right],$$

$$Z_\mu = \frac{a}{2h}\left[\frac{2(\mu - 1)}{(\eta - 1)} - 1 \right]. \tag{28}$$

In Fig. 2 we give graphically the temperature field as obtained from equation (28), due to symmetry, in one half of the workpiece. In this example we represent the heat source area by 27 point sources, distributed on the Z-axis. We recognize, except for the very vicinity of the source locations, a physically correct temperature field which, moreover, fulfills the adiabatic boundary conditions at the side and the top planes (15), (17), (18), as isotherms enter those planes perpendicularly. Moreover, the far-field boundary conditions for $Y \to +\infty$ (26) and for $X \to \pm\infty$ (12), (13) are fulfilled.

3.2. *Workpiece with adiabatic or isothermal bottom plane*

If we consider the table upon which the workpiece is positioned to be a poor conductor and/or the heat transfer between workpiece and table to be poor, the boundary condition at the bottom plane is expected to be close to adiabatic. In the above formulation (11)–(18) this situation corresponds to $Nu \to 0$. Physically, in such a situation the heat is removed dominantly by advection due to the source movement. We can construct a solution for the temperature field by using, once more, the 'method of images'. We get

$$\theta(X, Y, Z) = \frac{ad}{2\pi\omega\eta h^2} \sum_{\nu=1}^{\omega} \left\{ \exp\left[-\frac{Pe}{2}(X - X_\nu) \right] \times \sum_{\mu=1}^{\eta} \sum_{n=-\infty}^{+\infty} \sum_{m=-\infty}^{+\infty} \frac{\exp\left[-\frac{Pe}{2} R_{nm} \right]}{(\pm 1)^m R_{nm}} \right\},$$

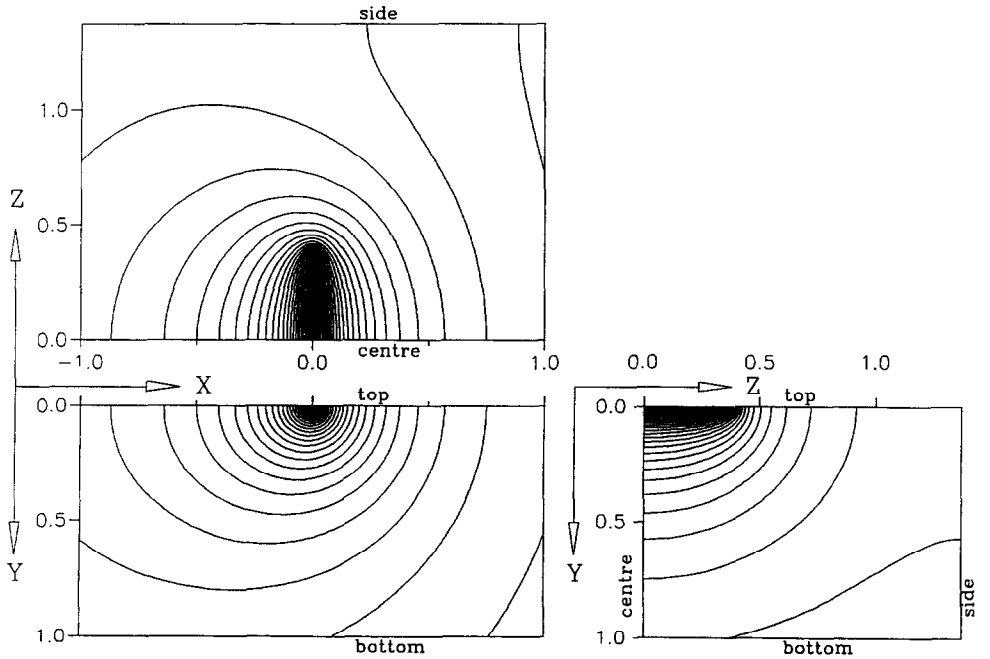

FIG. 2. Temperature field obtained for the workpiece of infinite thickness. Given are equally spaced isotherms using $\Delta\theta = 0.005$. Parameters are $Pe = 1$, $b/h = 11/4$, $d/h = 1/8$, $a/h = 3/4$. Number of sources are $\omega = 1$, $\eta = 27$, number of imaging planes is chosen to assure a relative error below 10^{-6}, which corresponds to $|n| \lesssim 10^3$.

with

$$R_{nm} = \left((X-X_\nu)^2+(Y-2m)^2+\left(Z-Z_\mu-\frac{b}{h}n\right)^2\right)^{1/2},$$

$$X_\nu = \frac{d}{2h}\left[\frac{2(\nu-1)}{(\omega-1)}-1\right],$$

$$Z_\mu = \frac{a}{2h}\left[\frac{2(\mu-1)}{(\eta-1)}-1\right]. \qquad (29)$$

In equation (29) the plus sign has to be used to obtain the adiabatic bottom plane. In Fig. 3 a corresponding plot of the isotherms is given by using an identical modelling of the heat source area as done in Fig. 2. It should be noted that the difference with respect to the temperature field in Fig. 2 is purely caused by the different boundary condition at the bottom plane. We recognize an adiabatic boundary as the isotherms enter the bottom plane perpendicularly.

By establishing an intense contact between the workpiece and a well-conducting table below, we approach a situation where the bottom plane of the workpiece is essentially forced to the constant ambient temperature T_∞. Clearly this case is included in our general formulation of the problem (11)–(18) by employing the limit $Nu \to \infty$. Under those circumstances the heat flux through the workpiece into the table becomes important and competes with the heat sink present due to advection. The scanning speed, or argued in dimensionless form the Peclet number Pe, will determine the balance of these two heat sinks: for small Pe heat will leave mainly through the bottom plane while for large Pe heat will be removed dominantly by advection.

In fact, the solution for the temperature field in the case of an isothermal bottom plane ($Nu \to \infty$) is included in equation (29) if we use the minus sign. The corresponding plot of the temperature field is given in Fig. 4. It should be noted that the isotherms are parallel to the bottom plane if one approaches this boundary.

3.3. *Workpiece with general heat transfer at the bottom plane*

We use a standard finite element code (FIDAP 6.0) to compute the temperature field in the most general case of arbitrary Nu. The three-dimensional calculations are done for one half of the workpiece, whereas the infinite extent in scanning direction X is simulated by using the computational range $-10 \leqslant X \leqslant 10$. Depending on the workpiece geometry we employ 20 000–30 000 nodes in 27-node brick elements and do the computations in non-dimensional variables, precisely according to the present formulation (11)–(18).

Figure 5 gives both a sketch of the elements used in the middle portion of the workpiece, as well as the temperature field obtained. In fact, the isotherms are given using identical spacing as employed within Figs. 2–4. It should be noted that the centre plane, the outer region of the top plane and the side planes of the workpiece exhibit adiabatic boundary conditions as

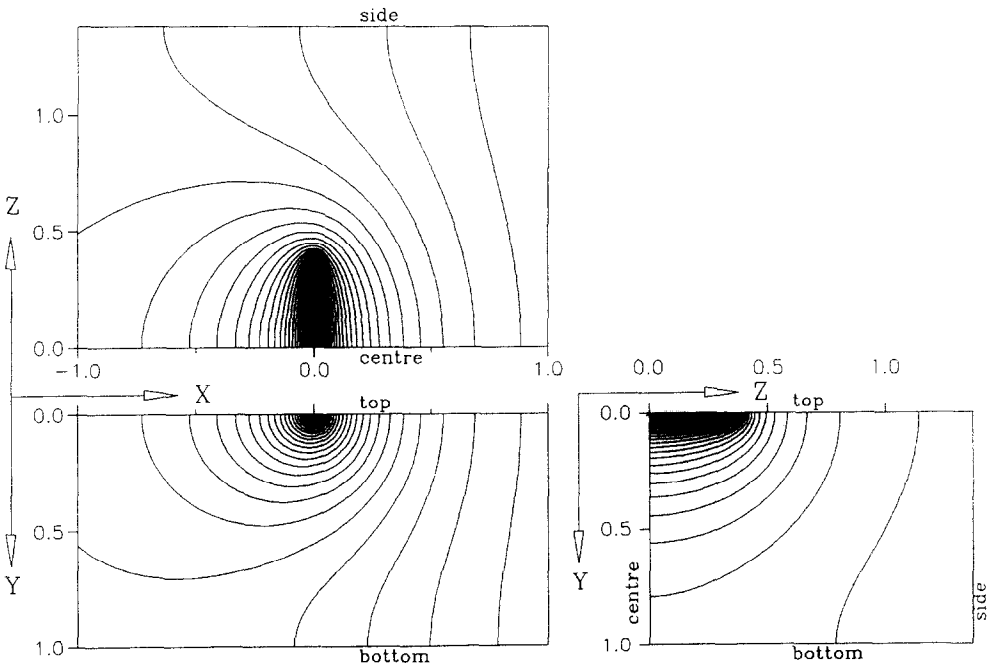

FIG. 3. Temperature field obtained for the workpiece with adiabatic bottom plane. Given are equally spaced isotherms using $\Delta\theta = 0.005$. Parameters are $Pe = 1$, $b/h = 11/4$, $d/h = 1/8$, $a/h = 3/4$. Number of sources are $\omega = 1$, $\eta = 27$, number of imaging planes is chosen to assure a relative error below 10^{-6}, which corresponds to $|n|, |m| \lesssim 10^3$.

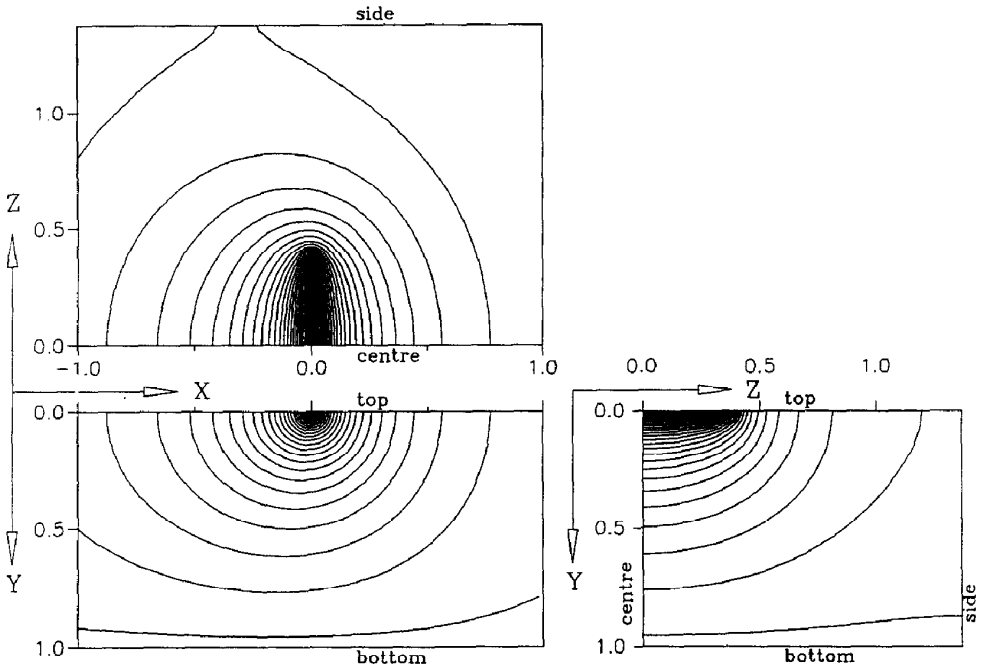

FIG. 4. Temperature field obtained for the workpiece with isothermal bottom plane. Given are equally spaced isotherms using $\Delta\theta = 0.005$. Parameters are $Pe = 1$, $b/h = 11/4$, $d/h = 1/8$, $a/h = 3/4$. Number of sources are $\omega = 1$, $\eta = 27$, number of imaging planes is chosen to assure a relative error below 10^{-6}, which corresponds to $|n|, |m| \lesssim 10^3$.

obvious from the perpendicular direction of the isotherms. In contrast the bottom plane features neither an adiabatic nor an isothermal boundary condition as isotherm directions depend on the local value of temperature. Thus, the Nusselt-type boundary condition with $Nu = 0.26$ is active. This particular Nusselt number has been taken from measurements when contacting a tool steel workpiece with a constant temperature copper table.

4. RESULTS FOR THE PENETRATION DEPTH

We now employ the models for the temperature field, developed in Section 3, to derive the penetration

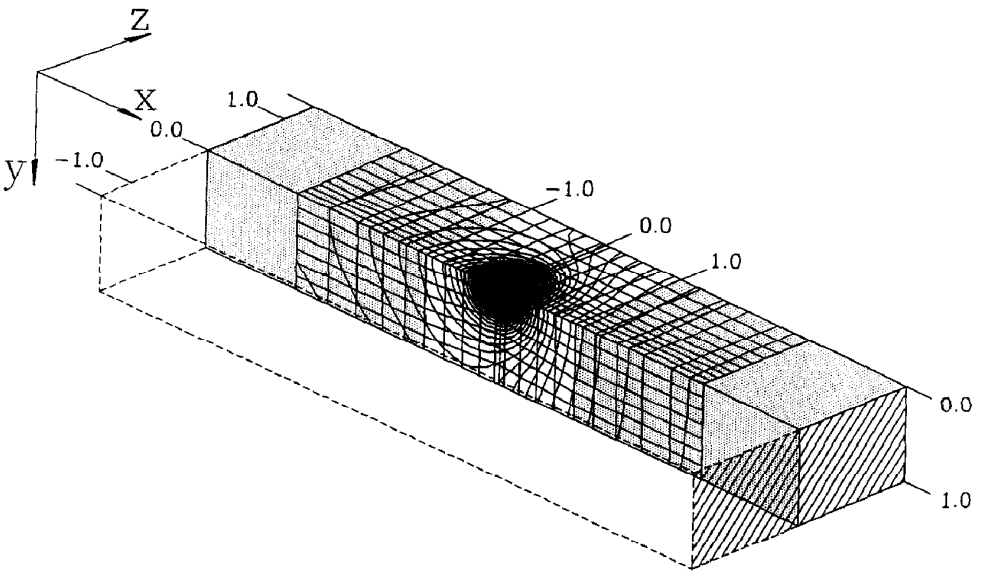

FIG. 5. Temperature field obtained for a workpiece with $Nu = 0.26$. Given are equally spaced isotherms using $\Delta\theta = 0.005$. Parameters are $Pe = 1$, $b/h = 11/4$, $d/h = 1/8$, $a/h = 3/4$.

depth of the temperature θ^* into the workpiece. As already discussed by using equation (23), besides geometry, we expect a dependency on Peclet number and Nusselt number. Figure 6 shows in a double-logarithmic diagram the dimensionless penetration depth t^*/h as function of Pe. The choice of parameters is motivated by an actual experiment wherein tool steel has been processed using a laser heat source (cf. Schüssler *et al.* [16]).

The solid curves connecting the symbols are numerical (FEM) results for two different heat transfer conditions at the bottom plane, namely (a) adiabatic ($Nu = 0$) and (b) including realistic heat losses towards the table ($Nu = 0.26$). We see that both of these curves collapse in a range of higher Peclet numbers $Pe \gtrsim 2$. Additionally for both curves we find $t^*/h \to 0$ as $Pe \to \sim 14$. Physically, this parameter range is dominated by an effective heat removal due to advection which for further increased scanning speeds (Pe) completely inhibits the penetration of the temperature θ^* into the workpiece.

By turning to the range of small Peclet numbers, we recognize two clearly distinguished solid lines depending on the heat transfer condition posed at the bottom plane. For the adiabatic boundary condition ($Nu = 0$) we get complete penetration ($t^*/h \to 1$) of the temperature θ^* as Pe decreases towards $Pe \cong 0.3$. In contrast, for realistic heat losses at the bottom plane ($Nu = 0.26$) a constant value of the penetration depth $t^*/h \cong 0.12$ is approached as $Pe \to 0$. The above results can be summarized as follows: for large Peclet numbers, featuring small penetration depths, the consideration of the bottom plane's heat transfer law is not really necessary. In contrast, for small Peclet numbers, featuring large penetration depths, the consideration of the bottom plane's heat transfer law is essential, since those heat losses dominate the process!

We now turn to the results from the analytical models (29) for the adiabatic and isothermal bottom plane which are incorporated in Fig. 6 as dashed and dotted lines. We consider a reasonable agreement of the curve obtained for adiabatic conditions (dashed) in the range of small Peclet numbers $Pe \lesssim 3$ with our corresponding numerical findings. Both curves predict a penetration through the complete workpiece for $Pe \cong 0.3$. In the range $Pe \gtrsim 3$, however, both curves diverge strongly as the analytical findings do not confirm $t^*/h \to 0$ for $Pe \cong 14$. This discrepancy is due to the modelling of the heat source area within the analytical solution (29) by means of a finite number of point heat sources. In detail the singularity of temperature, precisely at each single source position, implies a non-zero penetration depth of each temperature into the workpiece. The predictions based on these analytical solutions are therefore unphysical in the range of very small penetration depths. This range is shaded in Fig. 6.

Turning now to predictions for the isothermal bottom plane (dotted line) we find that the penetration depth approaches a constant value of $t^*/h \cong 0.06$ in the limit $Pe \to 0$. In the small Peclet number range, thus, the analytical curves for $Nu = 0$ and $Nu \to \infty$ provide an upper and a lower bound for the penetration depth to be obtained for arbitrary Nusselt number. This conjecture is in accord with our numerical predictions for $Nu = 0.26$, predicting a constant penetration depth of $t^*/h \cong 0.12$ in the limit $Pe \to 0$, i.e. within this respective interval.

It is useful to infer one further limit from Fig. 6. By employing the limit $Pe \to 0$ in conjunction with the finite thickness of the workpiece and a Nusselt-type boundary condition at the bottom plane, we can derive an upper bound for the penetration depth, which should hold for $Nu \cong 1$. We get

$$Pe \to 0: \quad \frac{t^*}{h} < \left\{ 2\pi \frac{h}{a} \frac{h}{d} \theta^* - (1 - Nu^{-1}) \right\}^{-1}, \tag{30}$$

which for the parameters of Fig. 6 yields $t^*/h < 0.116$. This value agrees reasonably with the asymptote of the $Nu = 0.26$ curve in Fig. 6. Equation (30) is strictly valid only for a single point source and $(1 - Nu^{-1}) \ll 1$, i.e. close to the semi-infinite case ($Nu = 1$).

Up to now we have discussed both the effect of Peclet number and Nusselt number. Equation (23) detects, moreover, a dependency on θ^*. For the sake

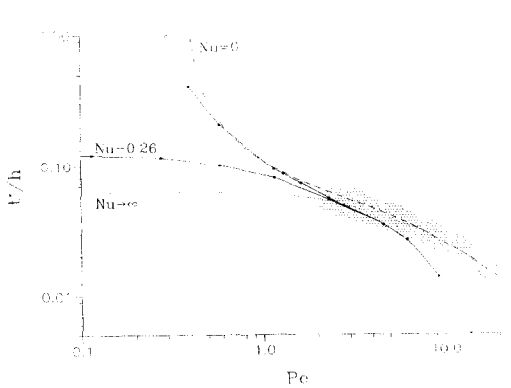

FIG. 6. Penetration depth of the temperature $\theta^* = 0.085$ as function of Peclet and Nusselt number. Geometry parameters are $b/h = 11/4$, $d/h = 1/8$, $a/h = 3/4$.

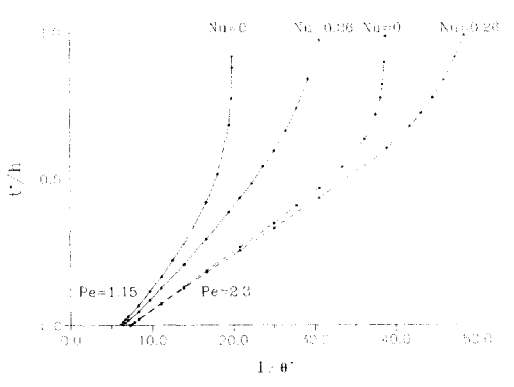

FIG. 7. Penetration depth as function of $1/\theta^*$. Constant parameters are $b/h = 11/4$, $d/h = 1/8$, $a/h = 3/4$. Solid curves are for $Pe = 1.15$, dashed curves for $Pe = 2.3$.

of simplified argumentation we plot in Fig. 7 the penetration depth as functions of the parameter $1/\theta^*$, for which

$$\frac{1}{\theta^*} = \frac{qh}{(T^* - T_\infty)\lambda} \tag{31}$$

holds. Thus, via equation (10), the abscissa is a dimensionless version of power density q. Given are FEM results for two different Peclet numbers, namely $Pe = 1.15$ (solid) and $Pe = 2.3$ (dashed), while again two different heat transfer conditions at the bottom plane are considered.

If we focus on the curves obtained for the higher scan speed (dashed), after exceeding a threshold value of $1/\theta^* = 7.2$–7.4, a linear increase of the penetration depth with power is predicted in the range $t^*/h < 0.5$ for both boundary conditions. As already concluded from Fig. 6, both boundary conditions lead to similar predictions if large Peclet numbers are present. Consequently, we find in Fig. 7 both dashed curves located close to each other, at least in the range $t^*/h < 0.5$. For larger values of the penetration depth ($t^*/h > 0.5$) the increase becomes clearly greater than linear and in the case of an adiabatic bottom plane ($Nu = 0$) even develops an asymptote as $t^*/h \to \infty$ for $1/\theta^* \to \sim 39$. Thus, the predictions resulting from both boundary conditions develop differently in this range. It should be borne in mind that the range of applications in 'surface processing technology' by definition restricts to small values of t^*/h and therefore the most important feature in Fig. 7 is the linear dependency on $1/\theta^*$, i.e. on power, in that respective range.

By turning to the curves obtained for the lower scanning speed (solid), we find the threshold values shifted towards $1/\theta^* = 6.1$–6.4 and the initial slopes of the curves clearly increased. The linear increase of t^*/h with $1/\theta^*$ is not as obvious, since, due to large slopes, it develops soon into an increase which is greater than linear. The curve obtained for an adiabatic bottom plane ($Nu = 0$) has its asymptote for a value of $1/\theta^* \cong 20$. Consistent with the findings from Fig. 6, both solid curves obtained for different boundary conditions at the bottom plane, now give greatly different predictions in the whole range of penetration depths as both curves diverge for increasing $1/\theta^*$. This is due to the smaller Peclet number which, via reduced advective effects, causes a stronger influence of the boundary condition at the bottom plane on the temperature field.

Next we address the influence of the geometrical parameters on the problem. In principle a departure from the two-dimensional, semi-infinite or infinite thickness cases arises for two reasons: (a) the extent of the heat source area in cross-track direction a is different from the width of the workpiece b. This situation can be viewed as a combination of two linked two-dimensional problems. In a 'near-field' heat will be confined in a slab of width a, while in a 'far-field' heat will be distributed across the whole width b of the workpiece. Thus, in between these two limiting cases, a truly three-dimensional heat flux has to be expected—heat migrates into the z-direction. (b) The thickness of the workpiece h is small, i.e. equation (27) is violated. This situation may still be two-dimensional if $a \sim b$ holds, but now the boundary condition at the bottom plane has a significant influence on the heat flow. This, in turn, means that any idealized boundary condition in this plane will reveal incorrect results.

In Fig. 8 we demonstrate with a set of calculations the transition between the truly three-dimensional problem, present for $b/h = 11/4$, $a/h = 3/4$, as it develops towards a two-dimensional problem, present for $b/h = a/h = 11/4$. The calculations are done for three different values of the parameter a/h, namely $a/h = 3/4, 5/4, 7/4$, while the total heat input $Q = qad$ and the parameters Nu, b/h, d/h are kept constant. Given is the penetration depth as function of the Peclet number Pe for two heat transfer conditions at the bottom plane, namely $Nu = 0, 0.26$.

We recognize two solid curves, valid for $a/h = 3/4$, which are already given in Fig. 6. As a/h is increased (compare dashed and dotted sets of curves), the 'far-field' predictions, i.e. predictions of large penetration depths, are in accordance for all cases as may be inferred from the common asymptote of the curves obtained for an adiabatic bottom plane ($Nu = 0$). Physically this means that heat is distributed across the whole workpiece width b and, thus, the width a of the heat source area is not relevant. This may be viewed as the two-dimensional 'far-field' problem.

In contrast, the 'near-field' predictions vary dramatically as, e.g. no penetration is predicted for $Pe \cong 14$, 2, 1.1 (0.3) if a/h is varied as $a/h = 3/4, 5/4, 7/4$. This reflects a strong change of the temperature field close to the heat input if a/h is varied, i.e. heat is essentially present in a slab of width a (just below the heat source area). This may be viewed as the two-dimensional 'near-field' problem.

Again we can characterize the range, where the

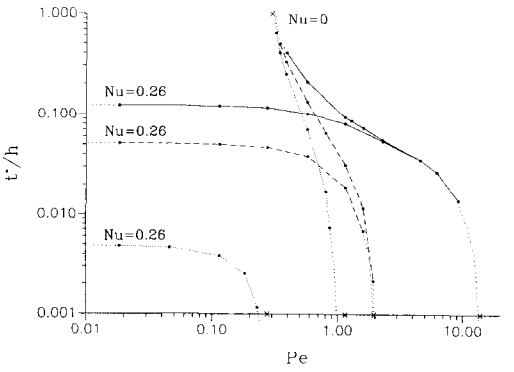

FIG. 8. Penetration depth of the temperature $T^* = 1420°C$ as function of Peclet number and geometry parameter a/h. Constant parameters are $b/h = 11/4$, $d/h = 1/8$, $Q = 390$ W. Solid curves are valid for $a/h = 3/4$, dashed curves for $a/h = 5/4$, dotted curves for $a/h = 7/4$.

boundary condition at the bottom plane does not influence the problem as $Pe \gtrsim 2$, while for smaller values of Pe the curves obtained for realistic ($Nu = 0.26$) and adiabatic ($Nu = 0$) boundary conditions depart strongly. This finding holds independently for all values of the geometry parameter a/h. All curves obtained for realistic boundary conditions at the bottom plane ($Nu = 0.26$) approach a constant value of t^*/h as $Pe \to 0$, namely $t^*/h = 0.12$, 0.051, 0.0048. Clearly, equation (30) is not able to capture the influence of a/h, since it employs a point source model (corresponding to the limit $a/h \to 0$) and, thus, in all cases $t^*/h < 0.116$ is obtained.

In summary we can view the geometry parameter a/h as responsible for the 'near-field' temperatures, i.e. for small penetration depth predictions. The values of a/h and b/h are, moreover, a reasonable measure for the three-dimensionality of the temperature field: if $a/b \cong 1$ holds, we have a two-dimensional problem present and as a/b departs further from unity towards $a/b < 1$ we approach a situation determined by a three-dimensional heat flow.

Finally, we focus on the variation of the workpiece thickness h which affects all dimensionless parameters, namely b/h, d/h, a/h, Pe and Nu. It allows us to demonstrate which differences result if either equation (27) holds (infinite thickness case) or if this equation is violated (finite thickness case). Given the parameters corresponding to the solid lines in Fig. 6, we can infer from equation (27)

$$h = 8\,\text{mm}: \quad U \gg 5.4\,\text{mm min}^{-1}, \tag{32}$$

whereas for a double thickness h we obtain

$$h = 16\,\text{mm}: \quad U \gg 1.3\,\text{mm min}^{-1}. \tag{33}$$

Thus, from equations (32), (33) it is obvious that the range of scanning speeds U for which the infinite thickness assumption is appropriate depends strongly on the thickness h: a large thickness h of the workpiece allows for a wider range of scanning speeds. It should be remarked here that we carry this particular discussion in terms of the original physical quantities rather than in dimensionless variables. A discussion in terms of dimensionless groups would, indeed, not be too transparent since h has been used as scaling length throughout all variables.

Figure 9 shows the results for the penetration depth t^* from our computations obtained for a thin workpiece ($h = 8$ mm) compared to the results obtained for a thick workpiece ($h = 16$ mm). We find that all curves collapse in the high scanning rate limit, proving that the infinite thickness assumption holds perfectly for high scanning speeds. In the case of the thin workpiece (solid lines) the curves for adiabatic ($k = 0$) and realistic ($k = 1000\ \text{W K}^{-1}\ \text{m}^{-2}$) boundary conditions depart for scanning speeds $U \lesssim 100$ mm min^{-1}, demonstrating the effect of the bottom plane's heat transfer law. Thus, the infinite thickness assumption is violated in that range. In contrast, the thick workpiece results (dashed lines) depart at lower scanning speeds,

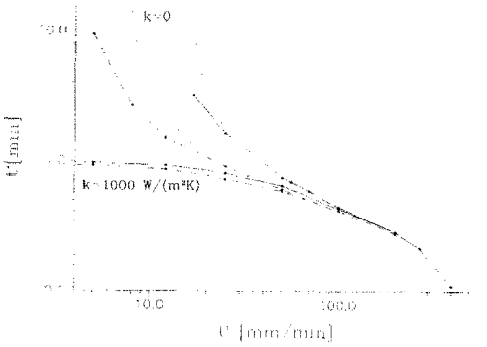

FIG. 9. Penetration depth of the temperature $T^* = 1420$°C as function of scanning speed U and workpiece thickness h. Constant parameters are $b = 22$ mm, $a = 6$ mm, $d = 1$ mm, $Q = 390$ W. Solid lines are valid for $h = 8$ mm, dashed lines for $h = 16$ mm. Dotted lines are results from the analytical approach with an adiabatic bottom plane for $h = 8/16$ mm.

namely for values $U \lesssim 40\,\text{mm min}^{-1}$. Therefore, in the case of a thick workpiece, a larger range of scanning speeds has to be considered for which the infinite thickness, assumption is appropriate. The increased thickness, therefore, is responsible for shifting the scanning speed limit below which the adiabatic and the realistic boundary conditions reveal different predictions, towards lower values of U. Clearly, the limit $h \to \infty$ leads to a situation where the adiabatic and the realistic predictions collapse within the complete range of scanning speeds. For this infinitely thick workpiece a secondary limit is of interest, namely $U \to 0$. This situation is physically characterized by a uniform distribution of heat in the z-direction due to large t^*. Therefore, a two-dimensional heat flow in an 'outer' region of the workpiece is left. From equation (28) we can infer the slope in that limit as

$$h \to \infty, U \to 0: \quad t^* \propto U^{-1}. \tag{34}$$

For validation of the numerical results obtained in particular for the adiabatic bottom plane ($k = 0$) we have added in Fig. 9 the analytical results (governed by equation (29)) as dotted lines. The asymptotes from both methods agree to a reasonable degree. Discrepancies, most obvious for the thick workpiece (dashed line), are caused by the finite length in x of the workpiece as present in the numerical model. It was checked for one single data point that a sufficient increase of the workpiece length in x within the numerical model leads to a prediction very close to the analytical curve. This, however, needs an increase of the number of nodes by a factor of up to ten. We therefore rely on the analytical curves which should hold perfectly in this particular range rather than performing costly computations converging to identical results.

5. RESULTS OBTAINED FOR THE PEAK TEMPERATURE

We finally turn to the prediction of the highest temperature, present on the centre line of the top plane

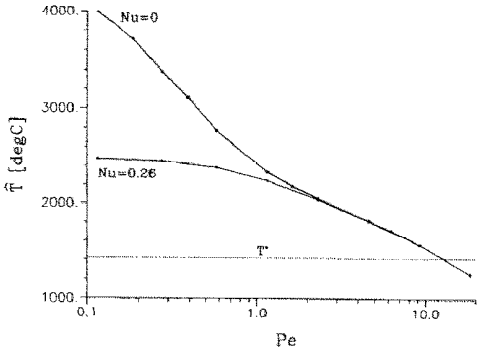

FIG. 10. Peak temperature $\hat{T}$ as function of Peclet and Nusselt number. Fixed parameters are $b/h = 11/4$, $d/h = 1/8$, $a/h = 3/4$, $Q = 390$ W.

of the workpiece. Clearly, the analytical approaches given in Sections 3.1 and 3.2 are not able to predict these data, since singularities in temperature are present. Thus we obtain all these data from FEM simulations (cf. Section 3.3). The identical set of parameters as already used for the penetration depth prediction in Fig. 6 is employed.

In Fig. 10 we present only one example demonstrating the dependency of peak temperature $\hat{T}$ on Peclet number Pe and Nusselt number Nu. Again for this quantity we recognize identical predictions, independent of Nu, in a range of high Peclet numbers $Pe \gtrsim 2$. In particular peak temperature falls below the respective penetration temperature T^* (cf. Fig. 6) at a value $Pe \cong 14$. This finding is consistent with our conclusions drawn from Fig. 6. By turning to the range of smaller Peclet numbers $Pe \lesssim 2$ we recognize that for the case of a realistic heat transfer at the bottom plane ($Nu = 0.26$) a peak temperature of $\hat{T} \cong 2500$°C is approached, which hardly depends on Peclet number in this range. In contrast, an adiabatic boundary condition at the bottom plane ($Nu = 0$) leads to a steep increase of peak temperature $\hat{T}$ if Peclet number is decreased. Of course, unbounded increase of $\hat{T}$ is only possible in the absence of radiative losses (as in our numerical model). Our computations are therefore expected to reveal unphysical results for very high workpiece temperatures—a more subtle modelling including radiative fluxes at least in the top plane would be required in such situations.

6. SUMMARY AND CONCLUSION

We have derived a set of finite-element and, in cases of meaningful limits, analytical models to predict the penetration depth of a specific temperature as well as peak temperature during processing of a brick-type workpiece. A rectangular heated area is applied to the top plane of the workpiece at constant scanning speed, while extents of workpiece and heat source area are modelled fairly generally. Predictions are strictly valid for conduction-dominated processes.

The adjustable parameters at the processing machine are obviously (i) the scanning speed U (in dimensionless form Pe) and (ii) the power density of the heat source (in dimensionless form $1/\theta^*$). If we focus firstly on the main dependency on Peclet number Pe (cf. Fig. 6), we find that penetration depth is independent of the thermal contact between workpiece and table (i.e. independent of Nu) if high Peclet numbers are considered. We find in the high Peclet number range penetration depth to decrease with increasing Pe until at some critical value of Pe zero penetration is predicted. For small Peclet numbers, however, the thermal contact of workpiece and table plays a crucial role as adiabatic conditions at the bottom plane lead to complete penetration while realistic heat transfer conditions for, e.g. steel and copper reveal constant penetration depth in the limit $Pe \to 0$. Thus, the thermal contact of workpiece and table controls the penetration depth for small Pe. This finding is probably of practical interest since the establishment of some desired thermal contact of workpiece and table is easily realized by, e.g. the choice of table material or introduction of intermediate layers such as graphite, etc. The goal during processing, of course, is to work with a 'smooth' dependency of the process result on the processing parameters and, simultaneously, achieve the highest possible output in terms of processed area. We shall subsequently term the dependency on processing parameters 'operation characteristic'. Under this aspect the thermal contact of workpiece and table seems to be one additional 'free' parameter to tailor a more ideal operation characteristic.

By varying geometry (cf. Fig. 9) we have further demonstrated that the Nusselt number is particularly effective in controlling the operation characteristic if relatively thin workpieces are processed. In contrast, thick workpieces tend to follow the predictions based on the infinite thickness assumption (independent of Nu) down to much lower values of the Peclet number. Thus, the range where a control of the operation characteristic is possible is limited to fairly low values of Pe in the case of thick workpieces.

A further possibility to influence the operation characteristic is the variation of cross-track size of the heat source area (cf. Fig. 8). In particular if the cross-track size a is small against the width b of the workpiece a truly three-dimensional heat flow leads to smaller slopes in the middle range of the $(t^*/h) = f(Pe)$ diagram when compared to a two-dimensional heat flow situation ($a = b$). Additionally the limit of operation where zero penetration is predicted is shifted towards higher values of Pe for small cross-track sizes. Of course, by reducing cross-track size, the output of the process in terms of processed area is likewise decreased and therefore the goals 'high process output' and 'smooth operation characteristic' are in conflict and a compromise needs to be achieved.

The peak temperature (cf. Fig. 10) is found to be likewise influenced by the Peclet number: an increase of Pe leads to decreasing peak temperatures. Additionally we find that the choice of the thermal contact of workpiece and table is a powerful tool

in restricting the peak temperatures in particular for small Peclet numbers. This, again, might be of interest from a practical point of view.

The dependency of the penetration depth on the second main parameter $1/\theta^*$, the net heat input, is now the focus. We find a mainly linear increase with $1/\theta^*$ in the typical range of applications (small penetration depth). The slope of these linear curves is determined by the Peclet number, i.e. we find large slopes for small Peclet numbers and vice versa. Here the goal of a smooth operation characteristic is readily obtained by the choice of high Peclet numbers in the actual process. Again the establishment of an intense thermal contact of workpiece and table (e.g. $Nu = 0.26$) provides a smoother operation characteristic if opposed to a poor thermal contact ($Nu = 0$). This is particularly true for larger values of the penetration depth.

REFERENCES

1. J. Mazumder, Laser heat treatment—the state of the art, *J. Metals* 18–26 (May 1983).
2. P. A. Molian, Engineering applications and analysis of hardening data for laser heat treated ferrous alloys, *Surf. Engng* **2,** 19–28 (1986).
3. D. Rosenthal, The theory of moving sources of heat and its application to metal treatments, *Trans. Am. Soc. Mech. Engng* **68,** 849–866 (1946).
4. H. S. Carslaw and J. C. Jaeger, *Conduction of Heat in Solids* (2nd Edn). Oxford University Press, Oxford (1959).
5. H. E. Cline and T. R. Anthony, Heat treating and melting material with a scanning laser or electron beam, *J. Appl. Phys.* **48,** 3895–3900 (1977).
6. M. F. Ashby and K. E. Easterling, The transformation hardening of steel surfaces by laser beams—I. Hypo-eutectic steels, *Acta Metall.* **32,** 1935–1948 (1984).
7. H. R. Shercliff and M. F. Ashby, The prediction of case depth in laser transformation hardening, *Metall. Trans.* **22A,** 2459–2466 (1991).
8. P. H. Steen, P. Ehrhard and A. Schüssler, Depth of melt-pool and heat affected zone in laser surface treatment, *Metall. Trans.* (in press).
9. R. Festa, O. Manca and V. Naso, A comparison between models of thermal fields in laser and electron beam surface processing, *Int. J. Heat Mass Transfer* **31,** 99–106 (1988).
10. R. Festa, O. Manca and V. Naso, Simplified thermal models in laser and electron beam surface hardening, *Int. J. Heat Mass Transfer* **33,** 2511–2518 (1990).
11. P. J. Timans, R. A. McMahon and H. Ahmed, Temperature distribution and molten zones induced by heating with line-shaped electron beams, *J. Appl. Phys.* **66,** 2285–2296 (1989).
12. S. Kou, D. K. Sun and Y. P. Le, A fundamental study of laser transformation hardening, *Metall. Trans.* **14A,** 643–653 (1983).
13. S. Kou, Welding, glazing, and heat treating—a dimensional analysis of heat flow, *Metall. Trans.* **13A,** 363–371 (1982).
14. C. Chan, J. Mazumder and M. M. Chen, A two-dimensional transient model for convection in laser melted pool, *Metall. Trans.* **15A,** 2175–2184 (1984).
15. H. Bornefeld, Das Temperaturfeld beim Verschweissen von Stahlblechen, *Techn. Zentralbl. Prakt. Metallbearb.* **43,** 14–18 (1933).
16. A. Schüssler, P. H. Steen and P. Ehrhard, Laser surface treatment dominated by buoyancy flows, *J. Appl. Phys.* **71,** 1972–1975 (1992).